Verification of Experimental Techniques for Flow Surface Determination

Cliff J. Lissenden
Pennsylvania State University
University Park, Pennsylvania

Bradley A. Lerch and John R. Ellis
Lewis Research Center
Cleveland, Ohio

David N. Robinson
University of Akron
Akron, Ohio

VERIFICATION OF EXPERIMENTAL TECHNIQUES FOR FLOW SURFACE DETERMINATION

Cliff J. Lissenden*
Pennsylvania State University
University Park, PA 16802

Bradley A. Lerch and John R. Ellis
National Aeronautics and Space Administration
Lewis Research Center
Cleveland, Ohio 44135

and

David N. Robinson
University of Akron
Akron, Ohio 44325

SUMMARY

The concept of a yield surface is central to the mathematical formulation of a classical plasticity theory. However, at elevated temperatures, material response can be highly time-dependent, which is beyond the realm of classical plasticity. Viscoplastic theories have been developed for just such conditions. In viscoplastic theories, the flow law is given in terms of inelastic strain rate rather than the inelastic strain increment used in time-independent plasticity. Thus, surfaces of constant inelastic strain rate or *flow surfaces* are to viscoplastic theories what yield surfaces are to classical plasticity.

The purpose of the work reported herein was to validate experimental procedures for determining flow surfaces at elevated temperature. Since experimental procedures for determining yield surfaces in axial/torsional stress space are well established, they were employed—except inelastic strain rates were used rather than total inelastic strains. In yield-surface determinations, the use of small-offset definitions of yield minimizes the change of material state and allows multiple loadings to be applied to a single specimen. The key to the experiments reported here was precise, decoupled measurement of axial and torsional strain. With this requirement in mind, the performance of a high-temperature multiaxial extensometer was evaluated by comparing its results with strain gauge results at room temperature. Both the extensometer and strain gauges gave nearly identical yield surfaces (both initial and subsequent) for type 316 stainless steel (316 SS). The extensometer also successfully determined flow surfaces for 316 SS at 650 °C. Furthermore, to judge the applicability of the technique for composite materials, yield surfaces were determined for unidirectional tungsten/Kanthal (Fe-Cr-Al).

INTRODUCTION

Many structural components are subject to multiaxial loading when in service. If such a component consists of elastoplastic or elastic-viscoplastic materials, a threshold surface is customarily used to distinguish irreversible response from reversible response. For elastoplastic materials, a yield surface, as defined by a yield criterion such as Tresca's (ref. 1) or von Mises' (ref. 2), can be used to delimit the elastic region in a given stress space (i.e., all points within the surface correspond to an elastic response). Once the current stress state reaches the yield surface, continued loading causes the yield surface to translate, expand, and/or distort. Elastic-viscoplastic material response is time-dependent by definition, and therefore, strain rates are used in constitutive theories. Flow surfaces for elastic-viscoplastic materials, which are surfaces of constant inelastic strain rate (SCISR's), are analogous to yield surfaces for elastoplastic materials. Sometimes the term flow surface is used to mean a surface of constant dissipation rate, but here the term *"flow surface"* shall be used to mean a SCISR.

---

*Summer Faculty Fellow at NASA Lewis Research Center.

To effectively and efficiently design structural components, we must use simplified theoretical constitutive models to describe material response; otherwise every component would have to be experimentally tested under every possible load condition. Classical plasticity theory as described by Hill (ref. 3) has been validated or invalidated for various materials through experimental testing (e.g., ref. 4). Many elastic-viscoplastic constitutive models have been developed in recent years (e.g., refs. 5 to 11). These models incorporate basic assumptions about material response that still must be verified for many important types of materials. Elastic-viscoplastic theories can be validated only by comparing experimental and theoretical results.

The objective of the work reported herein was to verify that current laboratory equipment and experimental techniques are sufficient to determine flow surfaces in axial/torsional stress space for materials at elevated temperature. First we compared current experimental techniques with previously established techniques for yield surface determination at room temperature. Verification was completed by actually conducting the flow surface determination tests at elevated temperature.

The key to experimental determination of flow surfaces at elevated temperature is the high-resolution, decoupled measurement of axial and torsional strains. Such measurement is difficult because of the coupling between the axial and torsional strains and because of the electronic noise from the heating system. In addition, these measurements must be made with extensometry because high-temperature strain gauges are still under development. For the experiments reported here, a multiaxial extensometer was used to conduct tests on 316 SS because of the wealth of data available for stainless steel (e.g., refs. 12 and 13). To show how well these techniques apply to composite materials, unidirectional tungsten/Kanthal (W/K), a ductile-fiber/ductile-matrix system having a reasonably strong fiber/matrix interfacial bond, was also tested.

Yield Surfaces

Yield and flow surfaces are defined in a particular stress space. Axial (σ_{11})/shear (σ_{12}) stress space is the most convenient for experimental determination because tubular specimens can be subjected to combined axial-torsional loading with relative ease. Further, if an isotropic or even an orthotropic material is used, the axial and torsional strains are decoupled. To experimentally determine a yield or flow surface, we must start in the elastic region and probe in enough directions to describe the shape and size of the surface. For this to be feasible, multiple probes should be conducted on a single specimen; otherwise, specimen-to-specimen variation and cost would overcome the usefulness of the technique. Hence, it is imperative that yield and flow surfaces be defined on the basis of a very small amount of inelastic deformation—so small, in fact, that any change in the material state is negligible.

Ellis et al. (ref. 12) conducted experimental studies of yield surfaces at room temperature using a small-offset strain definition of yield, $10 \mu\varepsilon = 10 \times 10^{-6}$ m/m, and multiple probes on a single specimen. Strain gauges measured axial and torsional strain. To detect yielding, the strains were combined by using an equivalent inelastic strain based on the second invariant of inelastic strain defined by

$$\varepsilon_e^{in} = \sqrt{\frac{1}{2} \varepsilon_{ij}^{in} \varepsilon_{ij}^{in}} \tag{1}$$

which is related to pure torsional loading and reduces to

$$\varepsilon_e^{in} = \sqrt{\frac{3}{4} \left(\varepsilon_{11}^{in}\right)^2 + \left(\varepsilon_{12}^{in}\right)^2} \tag{2}$$

for axial-torsional loading.

Flow Surfaces

The concept of a yield surface has less utility in viscoplasticity than it does in plasticity because viscoplastic theories admit stress states outside the yield surface, whereas classical plasticity theory does not.

Consequently, in viscoplastic theories the inelastic strain rate is continuous from the elastic regime to the inelastic regime, but in classical plasticity theory (ref. 14), it is discontinuous from the elastic regime onto the yield surface. A knowledge of the size and shape of surfaces of constant inelastic strain rate or flow surfaces is very useful, however, because it provides insight into how different combinations of loads affect the material state.

One class of viscoplastic theories (e.g., refs. 5, 8, and 10) is based on the evolution of internal state variables, and all theories in this class have the same mathematical structure (ref. 15). The total strain rate is the sum of the elastic and inelastic strain rates, that is,

$$\dot{\varepsilon}_{ij} = \dot{\varepsilon}_{ij}^{el} + \dot{\varepsilon}_{ij}^{in} \tag{3}$$

The inelastic strain rate is a function of the current stress and a set of internal state variables $\dot{\varepsilon}_{ij}^{in}(\sigma_{ij}Z_k)$. The internal state variables Z_k may be scalars or tensors (ref. 15). It is the internal state variables and their evolution that differentiate the various viscoplastic theories. Insight into this evolution can be obtained by comparing theoretical predictions with experimentally determined flow surfaces. Thus, experimental determination of flow surfaces is crucial to the continued development of elastic-viscoplastic models. These flow surfaces can be used to verify the evolution of the internal state variables even though not all viscoplastic theories (e.g., ref. 5) make use of the concept of a threshold surface.

EXPERIMENTAL PROCEDURE

Test Equipment

All experiments were conducted on a biaxial servohydraulic test machine having an axial load capacity of 222 500 N and a torsional capacity of 2 260 N-m. The tubular specimen is gripped by hydraulically actuated grips. The top grip of the load frame is attached to an axial-torsional load cell that is in turn attached to a crosshead, which remains fixed during a test. The bottom grip is attached to an actuator capable of independent rotational and vertical translational motions. The rotation of the actuator can be controlled in a closed-loop system by varying the angle of rotation, torque, and shear strain; its vertical translation is controlled by varying the displacement, load, or axial strain. Kalluri and Bonacuse (ref. 16) provide additional details regarding the biaxial test machine.

The test machine is equipped with an adjustable coil, 50-kW audiofrequency, induction-heating system (ref. 17) capable of temperatures in excess of 800 °C. For this reason, the specimen grips are water cooled. The specimen temperature is controlled by a thermocouple spot-welded to the gauge section of the specimen. To deter-mine the temperature distribution in the gauge section, eight thermocouples were spot-welded to the outer surface of the specimen. The temperature variation was controlled to ±1 percent of the target temperature (i.e., ±6.5 °C for isothermal testing at 650 °C). An enclosure around the test machine limited the effects of air currents.

Axial and torsional stress and strain data were saved electronically. In addition, three *x-y* recorders were used; one plotted the axial stress-strain response; one, the torsional stress-strain response, and the third, the probes in axial-torsional stress space.

Specimen Details

Type 316 stainless steel.—Specimens were fabricated from a single heat of 50.8-mm-diameter AISI type 316 SS bar stock. The composition and the room temperature properties reported by the manufacturer are shown in tables I and II, respectively. The material was heat treated by the manufacturer at 1038 °C for a sufficient time to dissolve precipitated carbides; then it was quenched in water.

Specimens were machined to have a 41-mm-long reduced gauge section with a nominal outer diameter of 26 mm and a wall thickness of 2 mm (fig. 1). After machining, each specimen was heat treated as follows: heated to 1065 °C in 2 hours in flowing argon (0.5 cf/hr); held for 30 min; cooled to 537 °C in 9 min; then continued cooling to room temperature. Details regarding the specimen microstructure and preparation can be found in reference 18.

Unidirectional tungsten/Kanthal.—One tubular $[0_6]$ composite specimen tested was composed of Kanthal (Fe-Cr-Al; see table III) reinforced with continuous 200-μm-diameter tungsten (218-W) fibers. Its nominal fiber volume fraction was 0.35. The specimen geometry was similar to that of the 316 SS specimen shown in fig-ure 1, except the nominal outer diameter was 25.4 mm and the wall thickness was 2.3 mm. Cross sections of the tubular specimen are shown in figure 2.

The tungsten/Kanthal (W/K) specimen was manufactured by using the hot isostatic press technique. Metallography conducted on the ends of the as-fabricated specimen revealed numerous cracks in the W fibers (fig. 2). These cracks were oriented circumferentially and occurred primarily in fibers in the innermost plies. Despite the pre-test damage, the W/K specimen was tested at room temperature to determine if the experimental techniques were applicable to metal matrix composites (MMC's).

Strain Measurement

As noted earlier, the key to conducting successful yield- and flow-surface experiments is the accurate measurement of axial and torsional strain at the microstrain level. Such high-resolution strain measurement is required not only to minimize the change in material state during testing but also to permit multiple probes of a yield or flow surface on a single specimen. Of the many factors affecting the high-resolution strain measurement, perhaps the most important are minimizing the electronic noise and decoupling the axial and torsional strains. Further, a high level of performance must be maintained at temperatures ranging from 20 to 1000 °C.

Multiaxial extensometer.—An off-the-shelf multiaxial extensometer (fig. 3) that can measure the axial and torsional strain over a wide range of temperatures was used in this investigation. The accuracy of the extensometer was verified by comparing its data with strain gauge data at room temperature. This extensometer contains two alumina rods 25 mm apart that are located on the specimen by indentations and the spring loading provided by a mounting fixture. The top rod is free to move only in the axial direction, whereas the bottom rod is free to move only in the circumferential direction. Axial displacement δ and the angle of twist θ are the output signals. The axial strain is

$$\varepsilon_{11} = \frac{\delta}{l_o} \tag{4}$$

and the torsional strain, which is assumed to be small, is

$$\gamma_{12} = \frac{r_o \theta}{l_o} \tag{5}$$

where r_o is the outer radius of the specimen and l_o is the gauge length (25 mm) of the extensometer. The tensorial shear strain is obtained from

$$\varepsilon_{12} = \frac{r_o \theta}{2l_o} \tag{6}$$

Strain gauge circuitry.—Four strain gauge rosettes (Micro Measurements EA-06-125RD-350) were mounted 90° apart around the midgauge of specimen #316SS18, which was tested at room temperature. The four longitudinal (0°) gauge arms were connected in a half bridge circuit (fig. 4) to average out any bending strains resulting from less than ideal specimen alignment. Two gauge arms oriented at +45° and two oriented at –45° were connected in a full bridge circuit (fig. 4) to provide an average tensorial shear strain signal. Both strain signals were amplified through dc signal conditioners.

Test Machine Control

All experiments were controlled by a 486-class microcomputer equipped with digital-to-analog (D/A) converters that provided independent control over the axial and torsional motions of the actuator (ref. 16). A multiplexed analog-to-digital (A/D) converter collected the load, torque, extensometer (axial and torsional), and strain gauge (axial and torsional) data. Software customized with FORTRAN programming issued

commands 100 times/sec to the D/A and A/D hardware. The acquired data were translated into axial and torsional stress-strain data with a 16-bit board and then written to an output file for postprocessing.

Two distinct types of test machine control were required to conduct the desired yield- and flow-surface experiments. The first controlled the *probing* of a yield or flow surface, and the second controlled the *preloading* applied to study the effects of this variable on subsequent yield or flow surfaces. *Preloading* was done in strain control, and *probing* was done in load (and torque) control. Hence, the test machine's dc controllers had to be manually shifted from strain to load mode between preloading and probing.

Two FORTRAN programs were written, one for determining yield surfaces and one for determining flow surfaces. Each program consisted of two basic elements. The first element was an optional preload sequence consisting of loading at a specified strain rate until a target stress or strain was reached; holding the strain constant for a time; and then unloading to a specified value of stress or strain. The second element was a sequence for probing the yield or flow surface at a specified equivalent stress rate,

$$\dot{\sigma}_e = \sqrt{\frac{3}{2} \dot{s}_{ij} \dot{s}_{ij}} \tag{7}$$

where $\dot{s}_{ij}$ are the deviatoric stress rates, which for axial-torsional loading reduces to

$$\dot{\sigma}_e = \sqrt{\dot{\sigma}_{11}^2 + 3\dot{\sigma}_{12}^2} \tag{8}$$

To minimize the effect of electronic noise, stresses and strains were averaged over a prescribed time period, usually 0.1 sec.

Every surface determination consisted of 16 unique probes conducted at different angles in axial-torsional stress space (fig. 5). The order in which the probes were conducted was chosen to maximize the difference between any two consecutive probe angles. The axial modulus E and the shear modulus G were determined by fitting a least-squares curve during a specified time period of each probe. The curve fit was typically initiated 20 to 30 sec into the probe to avoid the scatter around zero load (tables IV to VI).

After the elastic moduli were determined, inelastic axial and torsional strains were found by using

$$\varepsilon_{11}^{in} = \varepsilon_{11} - \frac{\sigma_{11}}{E}$$

$$\tag{9}$$

$$\varepsilon_{12}^{in} = \varepsilon_{12} - \frac{\sigma_{12}}{2G}$$

where ε_{11} and ε_{12} are the strains measured by the extensometer (or the strain gauges) and σ_{11} and σ_{12} are the measured stresses. For yield surface determination an equivalent inelastic strain

$$\varepsilon_e^{in} = \sqrt{\frac{2}{3} \varepsilon_{ij}^{in} \varepsilon_{ij}^{in}} \tag{10}$$

which is based on the second invariant of deviatoric stress, was calculated and compared with the yield criterion of 10 $\mu\varepsilon$ (10×10^{-6} m/m). Equivalent inelastic strain is related to pure axial loading and reduces to

$$\varepsilon_e^{in} = \sqrt{\left(\varepsilon_{11}^{in}\right)^2 + \frac{4}{3}\left(\varepsilon_{12}^{in}\right)^2} \tag{11}$$

for axial-torsional loading. To obtain equation (11), Poisson's ratio was taken to be 0.5. If the equivalent inelastic strain equaled or exceeded the yield criterion, unloading (at twice the loading rate) was initiated. For flow surface determination, the inelastic strain rate was calculated by determining the change in inelastic strain over a suitable time period:

$$\dot{\varepsilon}_{11}^{in} = \frac{\Delta \varepsilon_{11}^{in}}{\Delta t}$$

$$(12)$$

$$\dot{\varepsilon}_{12}^{in} = \frac{\Delta \varepsilon_{12}^{in}}{\Delta t}$$

Next, an equivalent inelastic strain rate was determined as in equation (11) and compared with a specified criterion of 100 $\mu\varepsilon$/min. The time increment Δt was chosen to minimize the effect of electronic noise on the calculated strain rates and to avoid adversely affecting the results.

Test Matrix

Prior to yield- and flow-surface testing, the performance of the extensometer was evaluated with respect to the resolution of the measured axial and torsional strains as well as its ability to decouple the two strains. To accomplish this, the extensometer was mounted on a tubular specimen that had the same geometry as the 316 SS tubes and that was instrumented with four strain gauge rosettes (as on 316SS18). Then the specimen was subjected to axial loading followed by torsional loading, to cause strains of the same order as those anticipated in the yield- and flow-surface tests. Thus, the resolution of the extensometer could be compared with that of the strain gauges and any coupling could be identified.

Eight runs, each consisting of 16 probes, were made to determine the initial yield surface of specimen 316SS18. Four runs used the extensometer-measured strains to detect yielding and four used the strain gauge data. Radial preloading, defined by $\sigma_{12} = \sigma_{11}/\sqrt{3}$, was then applied at the equivalent strain rate of $\dot{\varepsilon}_e = 300$ $\mu\varepsilon$/min until 50 percent beyond initial yielding. Four runs were made to determine the subsequent yield surface. Details of each yield-surface run on specimen 316SS18 are provided in table IV.

Initial flow surfaces for three 316 SS specimens were determined at 650 °C by using a time increment Δt of 10 sec and updating the inelastic strain rates and checking the flow criterion 10 times/sec. (Recall that data were acquired 100 times/sec, and then 10 sets of data were averaged together to yield 10 data sets/sec. Thus, 100 data sets were acquired in the 10 sec after determining the elastic moduli and before checking the initial flow criterion.) The effects of torsional preloading on subsequent flow surfaces were also investigated. Details of each flow surface run are shown in table V.

An attempt was made to determine the initial yield surface for W/K at room temperature. Unfortunately, a problem in the control software caused two preloads to be applied to the specimen during initial testing. Since the objective of the program was more to explore the viability of the experimental technique than to simply generate experimental results for W/K (which had already been damaged during fabrication), we decided to continue the test program in spite of the preloads. Four runs were made to determine the initial yield surface; then the specimen was heat treated (954 °C for 1 hr in vacuum) in an attempt to return it to its as-fabricated condition. Two more runs were made to determine the initial yield surface (table VI). Attempts to determine the initial flow surface at elevated temperature were inconclusive.

RESULTS AND DISCUSSION

Room Temperature

Both the resolution of the extensometer and the extent of any coupling between the axial and torsional strains were quantified prior to conducting yield-surface tests. While the torque was held to zero, tensile and compressive loads were applied (fig. 6(a)) to a specimen having the same geometry and strain gauge pattern as specimen 316SS18. Positive and negative torques were then applied while the axial force was held to zero (fig. 6(b)). In both cases the loads were limited to those producing strains in the range anticipated in the initial yield-surface tests for 316 SS (i.e., approximately 800 $\mu\varepsilon$).

Extensometer and strain gauge results are compared in figure 6. Under axial loading the resolution of the extensometer torsional strain signal was approximately 2 $\mu\varepsilon$, as defined by the vertical range between consecutive data points. The strain gauge torsional strain signal resolution, however, was approximately 1 $\mu\varepsilon$ (fig. 6(a)). Similarly, the resolution of the extensometer axial strain signal was approximately 1.5 $\mu\varepsilon$ and that of the strain gauges, less than 1 $\mu\varepsilon$ (fig. 6(b)).

The accumulation of apparent torsional strain with increasing axial strain, or vice versa, is frequently referred to as crosstalk. It can be caused by such things as misalignment of the extensometer with respect to

6

the direction of the load train because of improperly aligned indentations for the extensometer rods; an improperly seated rod in the indent; or mechanical imperfections inside the extensometer itself. Similarly, improper alignment of the strain gauges can cause crosstalk in the strain gauge data. Crosstalk was quite small (fig. 6) in the work reported here. Material anisotropy can cause a similar effect between axial and torsional strain, but in this case the coupling is actually in the material. Since the accumulated strain due to coupling was quite small (~5 $\mu\epsilon$) for any one type of loading, no corrections were applied, and thus the strains are used as measured.

Type 316 stainless steel.—The initial yield surface of 316 SS was determined by using both the extensometer and strain gauges. The results of eight runs, four with the extensometer and four with the strain gauges, are shown in figure 7. Typically, the first run is exploratory because the optimal duration of the time period for determining the elastic moduli in each probe is not known. Once the initial run has been made, the time period used to determine the elastic moduli is adjusted to provide the best estimate of the elastic moduli.

Runs 1 to 6 were made at an equivalent strain rate of 308 $\mu\epsilon$/min, while runs 7 and 8 were made at an equivalent strain rate of 555 $\mu\epsilon$/min (fig. 7). No significant difference was observed as a consequence of the different loading rates or as a result of run sequence. More importantly, no significant difference was observed between the runs in which the extensometer was used and the runs in which the strain gauges were used. Note that runs 1 to 5 were not the intended angles (see fig. 5). A correction was made after run 5, and all subsequent runs used the probe angles defined in figure 5.

The von Mises yield criterion (refs. 2 and 3) predicted the initial yield surface to be circular in the modified stress space shown in figure 7. The dashed line in figure 7 (parts (a) and (b)) represents a circle of radius 82 MPa overlaid on the data from runs 1 to 8. Notice that its center (–8 MPa, –4 MPa) is not located at the origin. This may be the result of residual stresses created during fabrication. The solid line in figure 7 represents the best fit of the data from runs 1 to 8 (as drawn with a french curve). It indicates that the experimentally determined yield surface has an oval shape and a center not located at the origin. The size and shape of the yield surface agree very well with those determined for 316 SS by Ellis et al. (ref. 12).

The elastic moduli determined from a least-squares curve-fit of typical extensometer (run 3) and strain gauge (run 2) results are compared in figure 8. For any probe angle, the maximum difference between the shear modulus measured by the extensometer and that measured by strain gauges was 1.8 GPa. The axial modulus exhibited more variation with probe angle and more variation between the extensometer and strain gauge results. These variations could be attributable to the axial strain signal fluctuations being larger than the torsional strain signal fluctuations, as will be discussed later. Nevertheless, the maximum difference between these measured axial moduli, as determined by the extensometer and the strain gauges, was only 17 GPa. These variations in the axial modulus had no apparent effect on the yield surface because the yield criterion is based on an offset from the elastic stress-strain response, not the elastic response itself.

The equivalent inelastic strain growth for probe 6 of an extensometer run 3 and strain gauge run 2 are shown in figure 9. The equivalent inelastic strain cannot be determined until after the elastic moduli are determined (i.e., after 70 sec) unless the data are postprocessed, which is not reported here. No significant difference is observed between the results from the extensometer and those from the strain gauges.

The Prandtl-Reuss flow law (refs. 19 and 20) associated with the von Mises yield criterion states that the inelastic strain increment is proportional to the deviatoric stress, that is,

$$d\varepsilon_{ij}^{in} = s_{ij}d\lambda \tag{13}$$

where $d\lambda$ is a constant, and implies that the direction of the inelastic strain increment is normal to the yield surface. The directions of the inelastic strain increments as determined by the extensometer (run 7) and strain gauges (run 8) are shown in figure 10. With few exceptions, the direction of the inelastic strain increment agrees reasonably well with the outward normal to the surface.

To study the performance of the extensometer under relatively large strains, radial preloading ($\sigma_{12} = \sigma_{11}/\sqrt{3}$) was applied until 50 percent beyond the initial yield, which was approximately 85 MPa for a probe angle of 45° in modified stress space. Axial and torsional stress-strain responses are shown in figure 11(a) for the applied preloading. No significant torsional hardening occurred; thus, it was necessary to use an equivalent stress criterion to stop preloading. Axial and torsional strains were held constant for 1 min before unloading to half the maximum values of the stresses. The results of two yield-surface runs in which the extensometer was used and two runs in which the strain gauges were used are shown in figure 11(b). Again, we noticed no significant differences between the extensometer and strain gauge results and no trends indicating a change in size or shape of the yield surface after preloading. However, the size, shape, and location of the yield surface after preloading (fig. 11(b)) were considerably different from the initial yield surface (fig. 7).

The direction of the plastic strain increment for each probe, as determined by the extensometer and strain gauge results, is shown in figure 12. Neither the extensometer nor the strain gauge results are in as good agreement with the normality condition as they were for the initial yield surface (fig. 10). Overall, the strain gauge results may be in slightly better agreement with the normality condition; however more data are needed to confirm this.

The experimental results presented in figures 7 to 12 indicate that the extensometer can adequately determine yield surfaces at room temperature. For the balance of the room-temperature experiments and all the elevated-temperature experiments, only the extensometer was used to measure strain.

Tungsten/Kanthal.—As previously mentioned, the W/K specimen was subjected to two significant preloads in the initial tests because of a problem with the control software. The first preload was negative torsion and the second was axial tension; however, the magnitudes of these preloads were unknown. Despite this, four runs were made to determine the yield surface (fig. 13(a)). In these runs the axial modulus was approximately 270 GPa, and the shear modulus was 104 GPa. The data exhibited a significant amount of scatter, but there was no evidence of translation or expansion of the yield surface between runs. An attempt was then made to remove the plastic deformation that occurred during the preloading and to restore the specimen to its as-fabricated condition, or close to it, by annealing for 1 hr at 995 °C in vacuum. After the annealing, two additional yield-surface runs were made at room temperature (fig. 13(b)). The heat treatment markedly reduced the scatter in the data. In figure 13(b) the data points for run 6 lie outside those for run 5 for 14 of the 16 probes; this suggests that the yield criterion of 10 $\mu\varepsilon$ may not be small enough to prevent a noticeable change in the material state of W/K.

Whether the heat treatment returned the W/K to its as-fabricated condition is uncertain. However, it seems reasonable to assume that the material state was at least close to the as-fabricated condition since the yield surface determined after annealing (fig. 13(b)) closely resembled the initial yield surface. In fact, if we consider the residual stresses created during fabrication, the initial yield surface we would predict for an MMC resembles the yield surface in figure 13(b). Tensile residual stresses in the matrix due to the mismatch between the coefficient of thermal expansion (CTE) of the fiber and the matrix suggest that the matrix will yield earlier in tension than in compression. Finally, a comparison of the yield surface after preloading but prior to annealing (fig. 13(a)) with that after annealing (fig. 13(b)) shows that the preloads caused the yield surface to expand in the directions of the preloads.

Elevated Temperature

The chief difficulty in conducting flow surface tests at elevated temperature is that heating systems can generate significant electronic noise. The differences between the strain signal at 21 °C and 650 °C for a 316 SS tube under zero load are shown in figure 14. It is quite evident that the noise level in both the axial and torsional strain signals is significantly higher at 650 °C than at 21 °C. Aside from the high frequency noise (~5 $\mu\varepsilon$), which is the difference between adjacent data points, there is a much larger amplitude (~20 $\mu\varepsilon$), low-frequency variation in the axial strain at 650 °C (fig. 14(a)). This variation could be associated with thermal strains due to small changes in temperature. The average CTE over the range between 21 and 650 °C was 20×10^{-6} °C^{-1}, with the CTE at 650 °C expected to be higher than the average. A ±0.5 °C change in temperature causes an axial strain of approximately ±10 $\mu\varepsilon$. In spite of the reduced resolution of the measured strain at elevated temperature, flow surfaces could still be determined.

The initial flow surface in modified stress space for one 316 SS specimen at 650 °C is shown in figure 15(a). Six runs were made to study the effects of repeated probing. The scatter in the data at each probe angle is reasonably small. The results from the six runs showed no significant trends with respect to the size, location, and shape of the flow surface. This suggests that the flow criterion of 100 $\mu\varepsilon$/min is small enough to prevent any significant change in material state. Figure 15(b) shows the specimen-to specimen variation in the initial flow surfaces for all three specimens tested. Again the scatter is reasonably small, aside from about eight extraneous points. Since there are 176 points shown in figure 15(b), these results are encouraging. The dashed line in figure 15 represents a circle of radius 54 MPa overlaid on the data from the three specimens tested. A french curve was used to draw the solid line to fit the data from all three specimens. The experimentally determined initial flow surface is elliptical in modified stress space and has its center located at (–4 MPa, –2 MPa).

The direction of the plastic strain increment for each probe angle is shown for runs 2 and 3 in figure 16. In many cases the direction of the plastic strain increment does not appear to be normal to the yield locus. However, in all cases it is pointed in the general direction of the outward normal.

The analog axial and torsional stress-strain responses obtained from the *x-y* recorders for each probe of run 4 (316SS22) are shown in figure 17. The pens were manually offset after every other probe in order to

8

prevent them from overwriting the previous results. There is a small permanent axial and/or torsional strain offset visible after every probe, indicating that the flow criterion was achieved because of material response rather than noise or apparent inelastic strain.

Preloading was applied to the 316 SS specimens to determine the effectiveness of the test procedures under large permanent strains at elevated temperature. To avoid possible complications associated with having both mechanical and thermal axial strains present during preloading, the applied preload was pure torsion. Torsional preloading up to the tensorial shear strain of 2500 $\mu\epsilon$ was applied to specimens 316SS22 and 316SS16 (fig. 18(a)); then they were partially unloaded, and flow surfaces were determined. Three subsequent flow surface determination runs were made for each specimen, the results of which are shown in modified stress space in figure 18(b). Scatter in the data is minimal, and compared to the initial flow surface (fig. 15), the subsequent flow surface has translated and elongated in the direction of the preloading (positive torsion).

It is important to note that the flow surfaces shown in figures 15 and 18 are not solely a function of the flow criterion of 100 $\mu\epsilon$/min, but depend on the time increment used to calculate the inelastic strain rates (10 sec). The time increment had to be large enough to minimize the effect of the electronic noise from the heating system (fig. 14). For example, if the amplitudes of the electronic noise were known to be 5 and 2 $\mu\epsilon$ for axial and torsional strain, respectively, and if a time increment of 1 sec was chosen, the apparent equivalent inelastic strain rate would have been 165 $\mu\epsilon$/min in the elastic region. However, if a time increment of 10 sec were used for the same noise levels, the apparent equivalent inelastic strain rate would have been 16.5 $\mu\epsilon$/min, a much more reasonable value. Thus, the flow surface indirectly depends on the amount of noise in the system.

There are two fairly obvious solutions to the electronic noise problem, the first being to eliminate, or at least significantly reduce, the noise by using filters or a different heating system. The second solution is to de-emphasize the importance of the flow surface results determined in real time and to manipulate the stored data by using curve-fitting techniques to smooth the data; then the flow surfaces can be determined from the smoothed data. Both avenues are currently being explored and results will be reported at a later date.

CONCLUDING REMARKS

Yield surfaces were experimentally determined for 316 SS tubular specimens at room temperature in axial-torsional space by using a 10-$\mu\epsilon$ definition of yield. All tests were controlled and all data acquired by custom computer software. Strain was measured by strain gauges and a multiaxial extensometer designed for use at high temperature. A comparison of yield surfaces determined with the extensometer and those determined with the strain gauges revealed that the extensometer has sufficient resolution to measure axial and torsional strain at the microstrain level, as required for this program. Further comparison of the current results with those reported in the literature (ref. 12) showed extremely good agreement for the size, shape, and location of the initial yield surface as well as for the yield surface following radial preloading to 50 percent beyond initial yielding.

Flow surfaces were determined for 316 SS at 650 °C by using a constant inelastic strain rate of 100 $\mu\epsilon$/min for the flow criterion. Electronic noise created by the induction heating system made it necessary to use a relatively large time increment in the calculation of the inelastic strain rates. Thus, the flow surfaces are an implicit function of the electronic noise in the system. It is therefore desirable to remove the electronic noise by filtering it out in real time during the test or by postprocessing the raw test data. Both methods are currently being explored.

FUTURE WORK

Future work will focus on determining the various types of inelastic surfaces: threshold, yield, surface of constant inelastic strain rate, and surface of constant dissipation rate for metal matrix composites at elevated temperature and on further refining the procedure for determining inelastic strain rate.

ACKNOWLEDGMENTS

REFERENCES

1. Tresca, H.: Memoire sur l'Ecoulement des Corps Solides. Memoires presentes par divers savants, vol. 18, 1868, pp. 733–799.
2. Von Mises, R.: Mechanik der plastischen Formänderung von Kristallen, Z. Angew. Math. und Mech., vol. 8, 1928, pp. 161–185.
3. Hill, R.: The Mathematical Theory of Plasticity. Oxford University Press, Oxford, 1983.
4. Taylor, G.I.; and Quinney, H.: The Plastic Distortion of Metals. Philos. Trans. R. Soc., vol. 230, 1932, pp. 323–362.
5. Bodner, S.R.; and Partom, Y.: Constitutive Equations for Elastic-Viscoplastic Strain-Hardening Materials. J. Appl. Mech, vol. 42, June 1975, pp. 385–389.
6. Miller, A.: An Inelastic Constitutive Model for Monotonic, Cyclic, and Creep Deformation: Part I - Equations Development and Analytical Procedures. J. Eng. Mater. Tech., vol. 98, Apr. 1976, pp. 97–105.
7. Chaboche, J.L.: Viscoplastic Constitutive Equations for the Description of Cyclic and Anisotropic Behaviour of Metals. Acad. Pol. Sci. Bul. Ser. Sci. Tech., vol. 25, no. 1, 1977, pp. 33–39, 42–48.
8. Robinson, D.N.: A Unified Creep-Plasticity Model for Structural Metals at High Temperature. ORNL TM–5969, 1978.
9. Freed, A.D.; and Walker, K.P.: A Viscoplastic Theory With Thermodynamic Considerations. Acta Mech., vol. 90, 1991, pp. 155–174.
10. Majors, P.S.; and Krempi, E.: Recovery of State Formulation for the Viscoplasticity Theory Based on Overstress. High Temperature Constitutive Modelling - Theory and Application, vol. 26, ASME, New York, 1991, pp. 235–250.
11. Arnold, S.M.; Saleeb, A.F.; and Castelli, M.G.: A Fully Associative, Nonisothermal, Nonlinear Kinematic, Unified Viscoplastic Model for Titanium Alloys. NASA TM–106926, 1995.
12. Ellis, J.R.; Robinson, D.N.; and Pugh, C.E.: Time Dependence in Biaxial Yield of Type 316 Stainless Steel at Room Temperature. J. Eng. Mater. Tech., vol. 105, Oct. 1983, pp. 250–256.
13. Bonacuse, P.J.; and Kalluri, S.: Results of In-phase Axial-Torsional Fatigue Experiments on 304 Stainless Steel. NASA TM-101464, 1989.
14. Freed, A.D.; and Walker, K.P.: Viscoplastic Model Development With an Eye Toward Characterization. J. Eng. Mater. Tech., vol. 117, Jan. 1995, pp. 8–13.
15. Bass, J.M.; and Oden, J.T.: Adaptive Finite Element Methods for a Class of Evolution Problems in Viscoplasticity. Int. J. Eng. Sci., vol. 25, no. 6, 1987, pp. 623–653.
16. Kalluri, S.; and Bonacuse, P.J.: A Data Acquisition and Control Program for Axial-Torsional Fatigue Testing. Applications of Automation Technology to Fatigue and Fracture Testing, American Society for Testing and Materials, 1990, pp. 269–287.
17. Ellis, J.R.; and Bartolotta, P.A.: Adjustable Induction-Heating Coil, NASA Tech Briefs, vol. 14, no. 11, Nov. 1990, p. 50.
18. Bonacuse, P.J.; and Kalluri, S.: Axial-Torsional Fatigue: A Study of Tubular Specimen Thickness Effects. J. Test. Eval., vol. 21, no. 3, May 1993, pp. 160–167.
19. Prandtl, L.: Spannungsverteilung in Plastischen Körpern. Proceedings of the First International Congress for Applied Mechanics, C.B. Biezeno; and J.M. Burgers, eds., Technische Boekhandel en Druckerij, J. Waltman, Jr., Delft, 1925, pp. 43–54.
20. Reuss, A.: Berücksichtigung der elastischen Formänderung in der Plastizitätstheorie. Z. Angew. Math. Mech., vol. 10, 1930, pp. 266–274.

TABLE I.—COMPOSITION OF TYPE 316 STAINLESS STEEL [From ref. 18.]	
Element	Content, wt %
C	0.04
Mn	1.75
P	.030
S	.013
Si	.57
Ni	10.20
Cr	17.70
Mo	2.08
Co	.19
Cu	.28
N	.067
Fe	67.08

TABLE II.—ROOM TEMPERATURE MATERIAL PROPERTIES OF TYPE 316 STAINLESS STEEL [From ref. 18.]

Yield strength, MPa 521
Ultimate tensile strength, MPa 661
Elongation, percent 44
Reduction in area, percent . . . .
78
Hardness, BHN[a] 207

[a]Brinell hardness number.

TABLE III.—COMPOSITION OF KANTHAL	
Element	Content, wt %
C	0.04
Cr	21.0
Al	5.8
Fe	73.16

TABLE IV.—TEST MATRIX FOR 316SS18 AT ROOM TEMPERATURE

Run	Axial-torsional loading, $\dot{\sigma}_e$, MPa/sec	Elastic moduli curve-fit time	
		Start time, t_1, sec	End time, t_2, sec
Without radial preload			
1[a]	1.00	10	50
2[a]		20	70
3[b]			
4[a]			
5[b]			
6[b]			
7[b]			
8[a]	1.67	12	42
	1.67	12	42
With radial preload			
9[b]	1.67	5	35
10[a]	1.00	5	55
11[b]	1.00	10	50
12[a]	1.00	10	50

[a]Strain measured by strain gauge.
[b]Strain measured by extensometer.

11

TABLE V.—TEST MATRIX FOR 316 SS AT 650°

[All strains measured by extensometer.]

Run	Axial-torsional loading, $\dot{\sigma}_e$, MPa/sec	Elastic moduli curve-fit time	
		Start time, t_1, sec	End time, t_2, sec
316SS22 without preload			
1	0.72	20	50
2		30	70
3	↓	30	70
4		30	70
5	1.43	15	35
6	1.43	15	35
316SS22 with torsional preload to 2500 $\mu\varepsilon$			
7	0.72	20	40
8	.72	30	60
9	.72	30	60
316SS16 without preload			
1	0.72	20	50
2	.72	30	60
3	.72	30	60
316SS16 with torsional preload to 2500 $\mu\varepsilon$			
4	0.72	30	60
5	.72	30	70
6	.72	30	70
316SS21 without preload			
(a)	0.72	30	60
1	.72	30	70
2	.72	30	70

[a] Probe at 90° and 270° (± torsion) only.

TABLE VI.—TEST MATRIX UNIDIRECTIONAL TUNGSTEN/KANTHAL (W/K)

[All strains measured by extensometer.]

Run	Axial-torsional loading, $\dot{\sigma}_e$, MPa/sec	Elastic moduli curve-fit time	
		Start time, t_1, sec	End time, t_2, sec
Initial yield surface at 21 °C			
1	1.67	20	60
2			
3	↓	↓	↓
4			
After heat treating (955 °C for 1 hr in vacuum)			
5	1.67	20	60
6	1.67	20	55

12
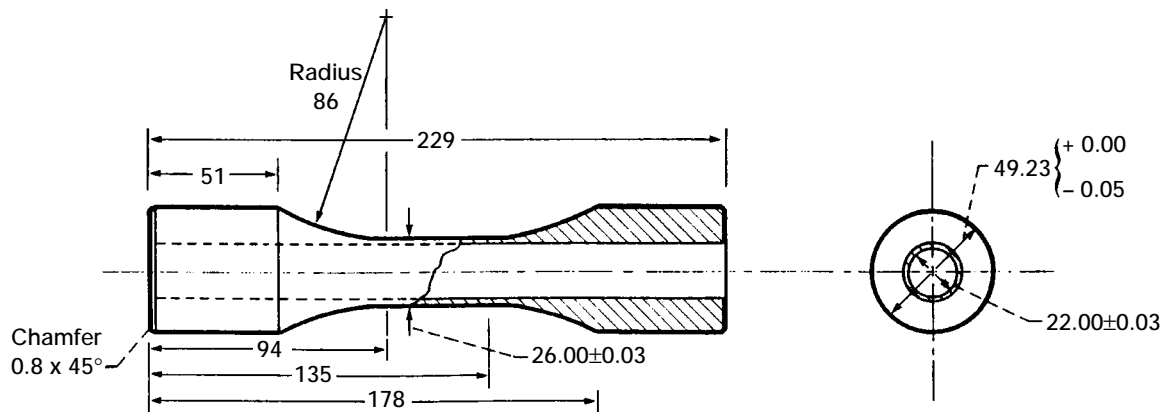
Figure 1.—Specimen geometry (all dimensions are in millimeters).
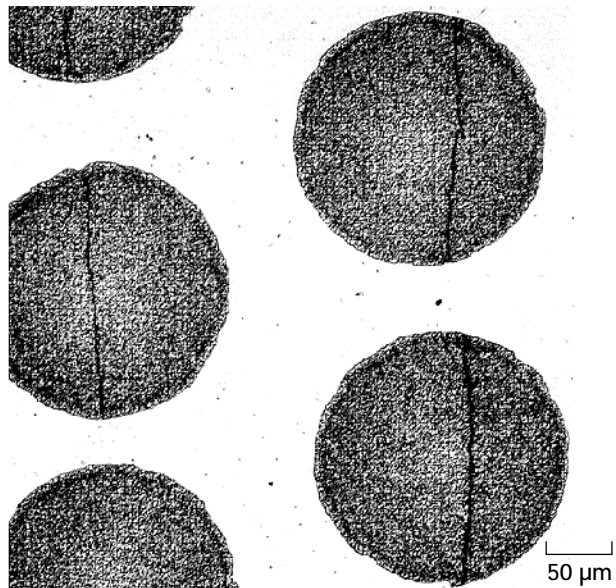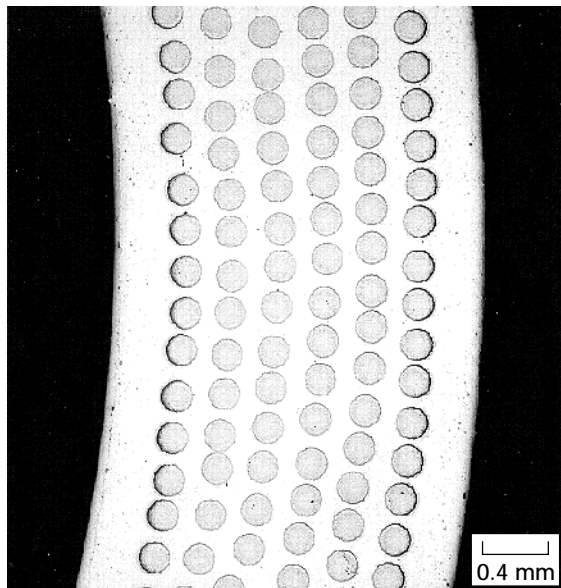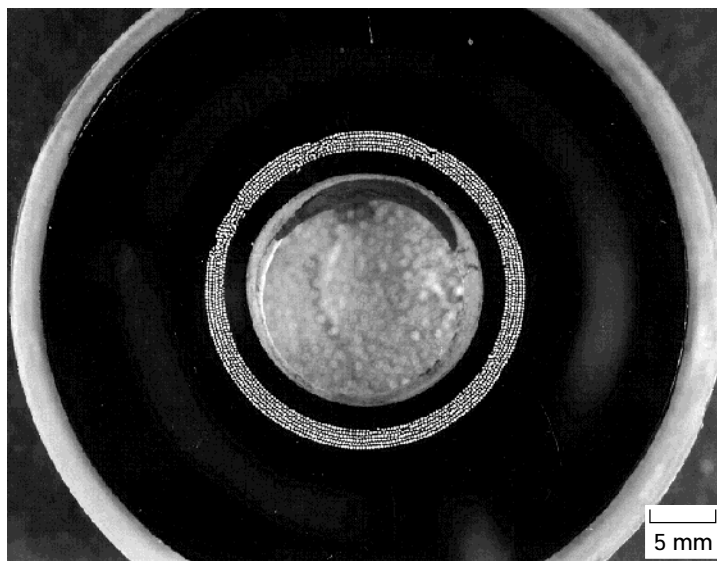
Figure 2.—Tungsten/Kanthal cross section.
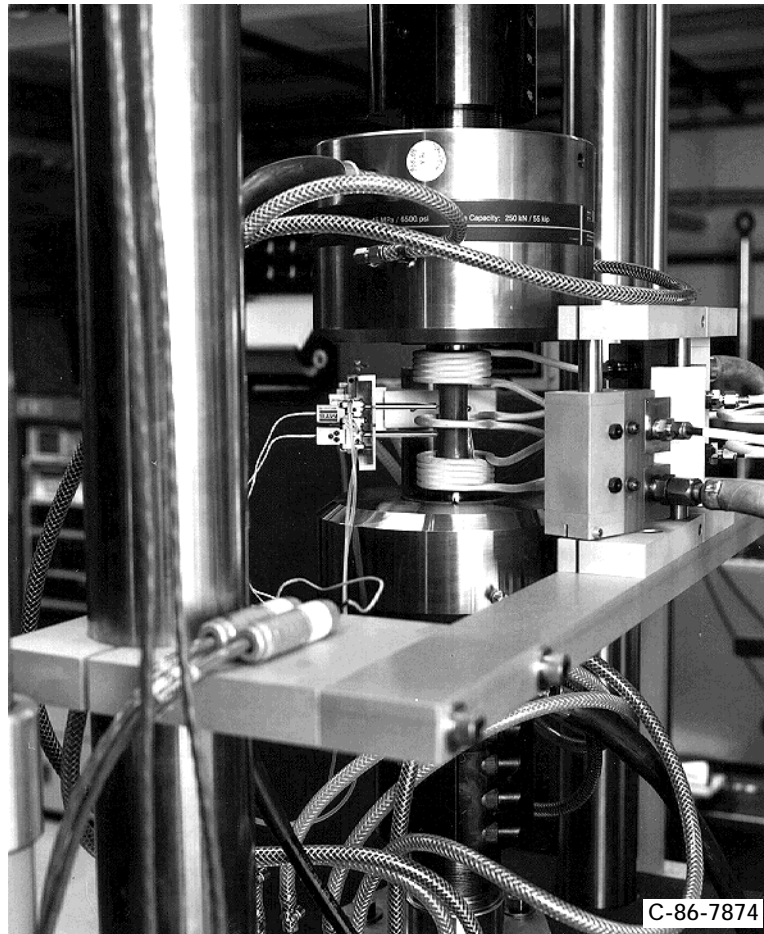
Figure 3.—Multiaxial extensometer.
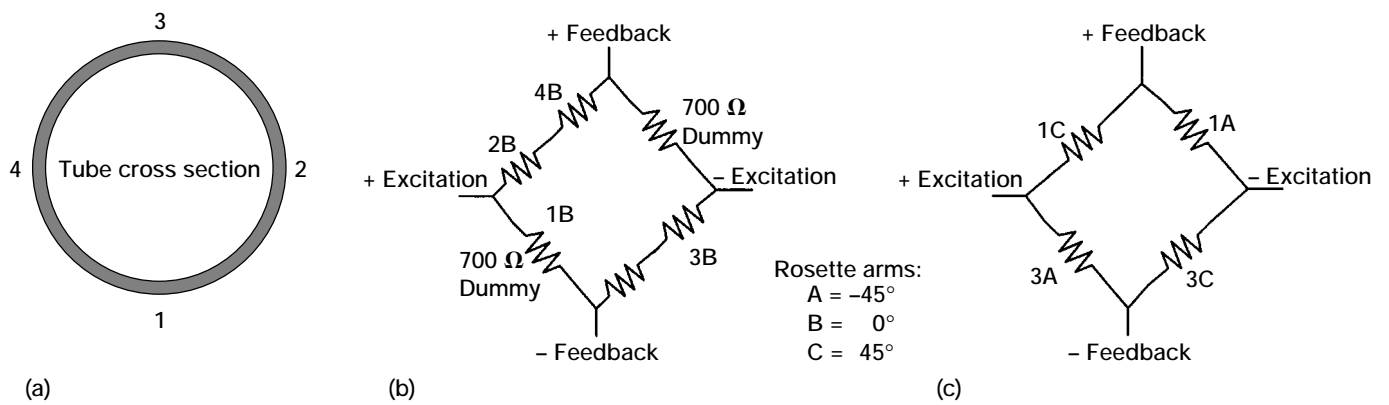
Figure 4.—Strain gauge circuitry. (a) Strain gauge rosettes. (b) Axial strain, half bridge. (c) Shear strain, full bridge.
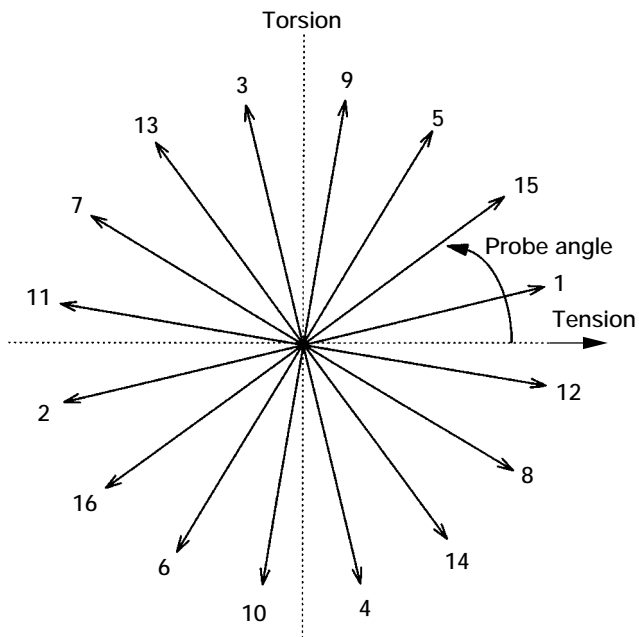
Probe number	Probe angle, deg.	Probe number	Probe angle, deg.
1	12	2	192
3	102	4	282
5	57	6	237
7	147	8	327
9	79	10	260
11	170	12	350
13	125	14	305
15	35	16	215

Figure 5.—Probes for determination of yield and flow surfaces.
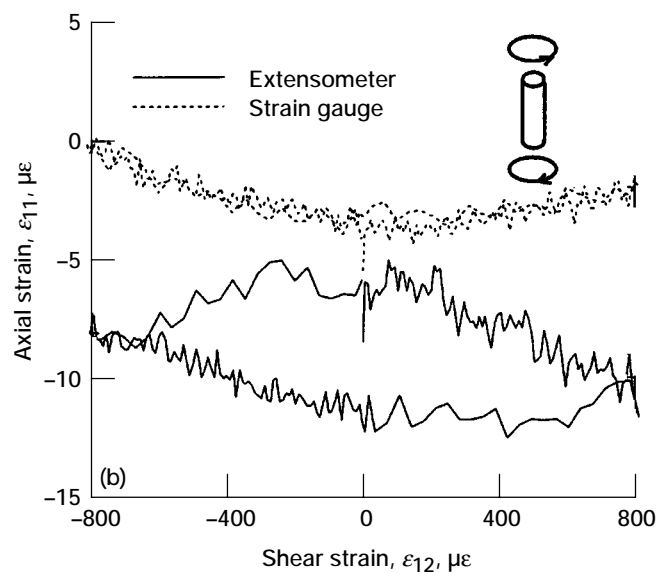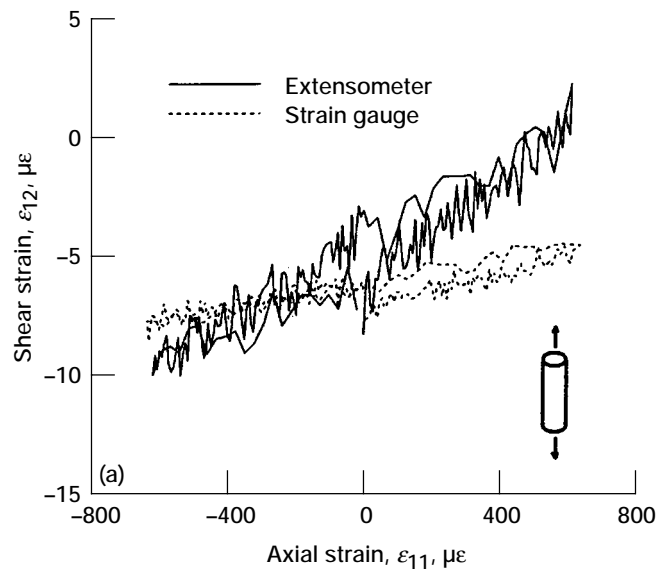
Figure 6.—Extensometer resolution and apparent strain. (a) Axial loading. (b) Torsional loading.

(a)
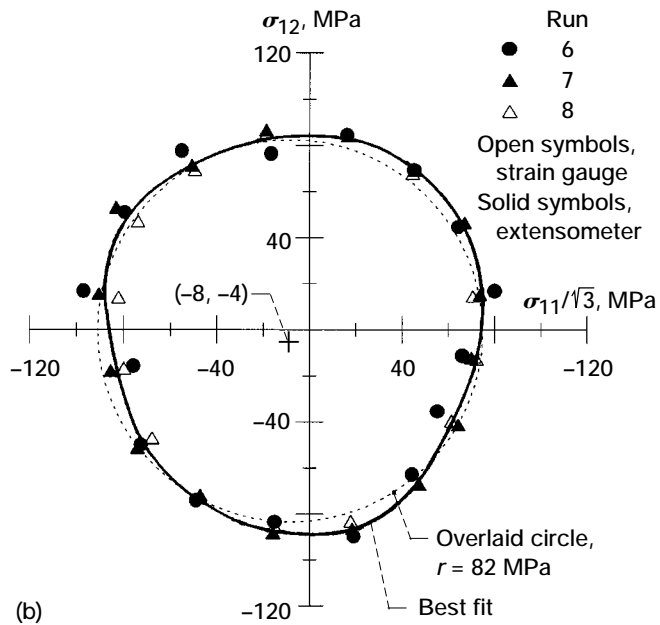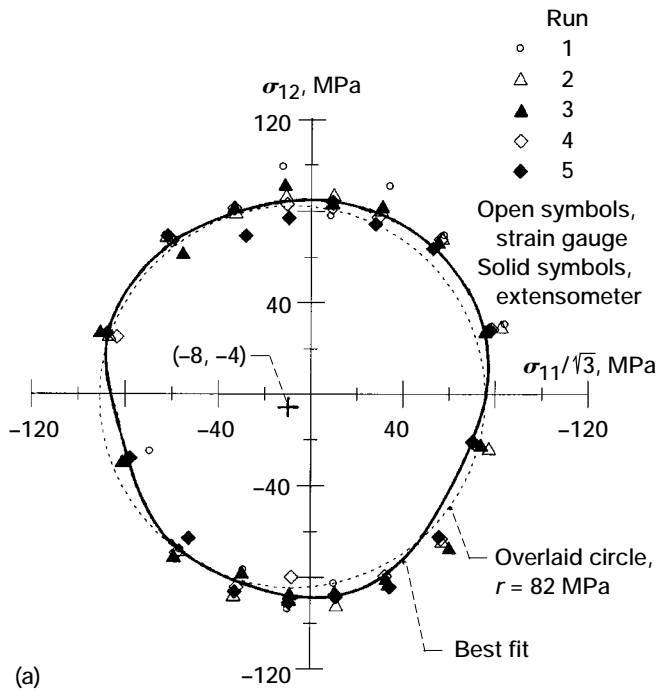
Figure 7.—Initial yield surface at 21 °C for sample 316SS18. (a) Runs 1 to 5, all at 308 με/min. (b) Run 6 at 308 με/min and runs 7 and 8 at 555 με/min.

(b)
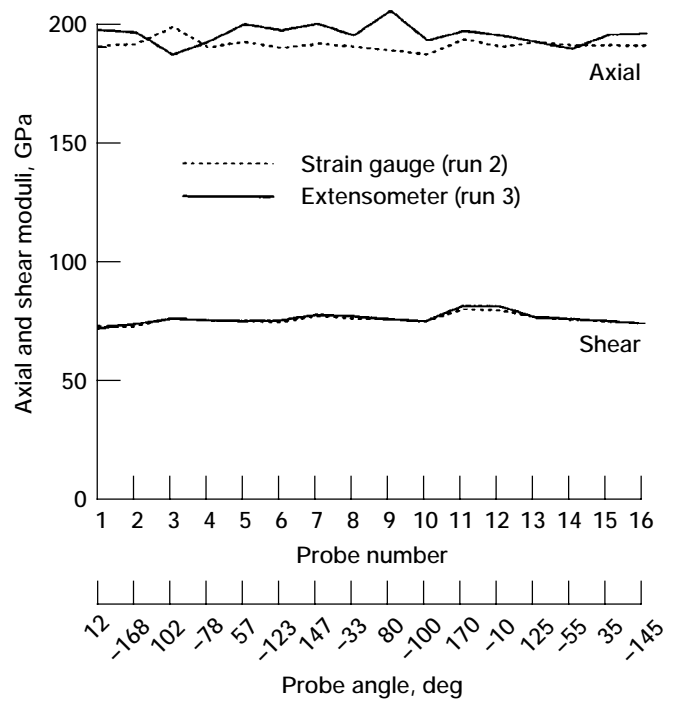
Figure 8.—Elastic moduli of 316SS18.
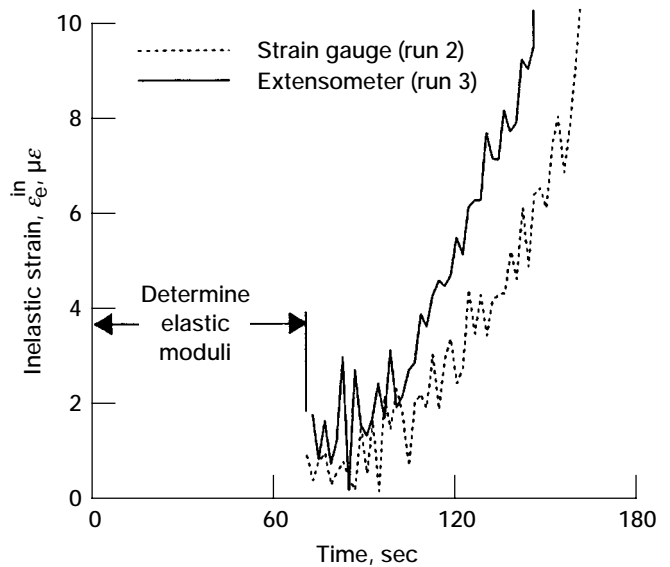
Figure 9.—Equivalent inelastic strain of 316SS18 at probe 6.
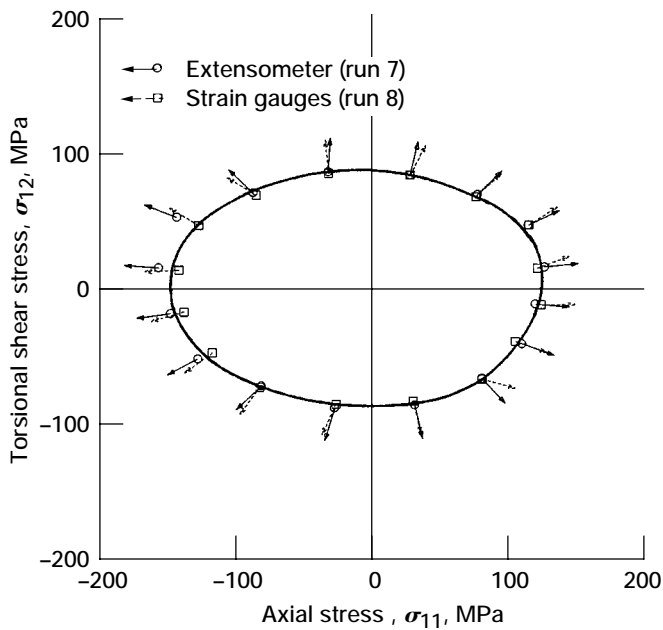
Figure 10.—Direction of inelastic strain increments for 316SS18.

(a)

(b)
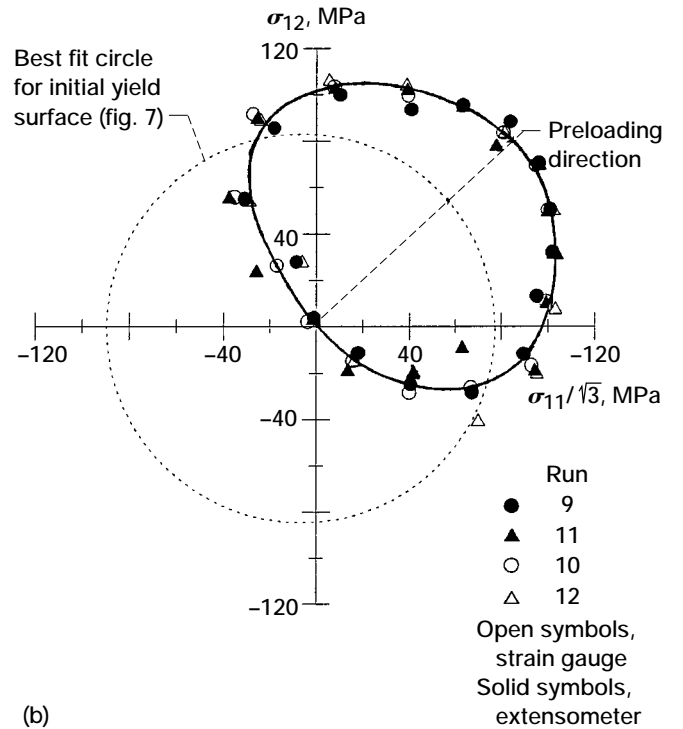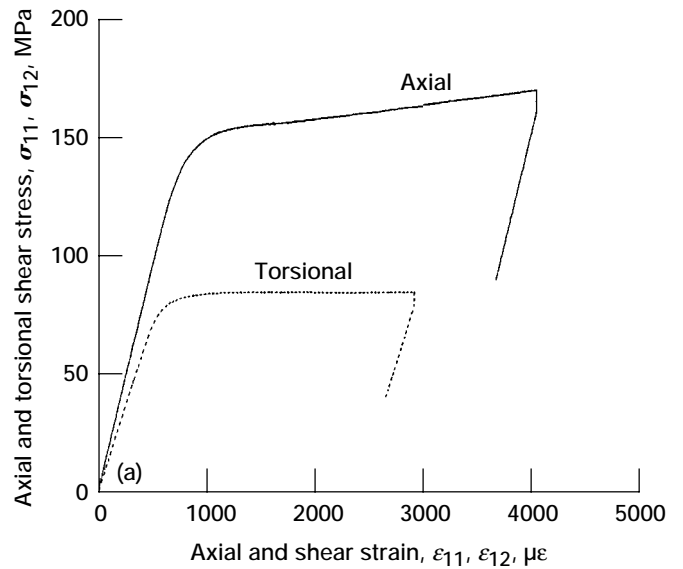
Figure 11.—Radial preload and subsequent yield surface for 316SS18. (a) Radial preloading applied to 316SS18 to 50 percent beyond initial yield ($\dot{\varepsilon}_e$ = 300 με/min). (b) Subsequent yield surface for run 9 at 555 με/min and runs 10 to 12 at 308 με/min.
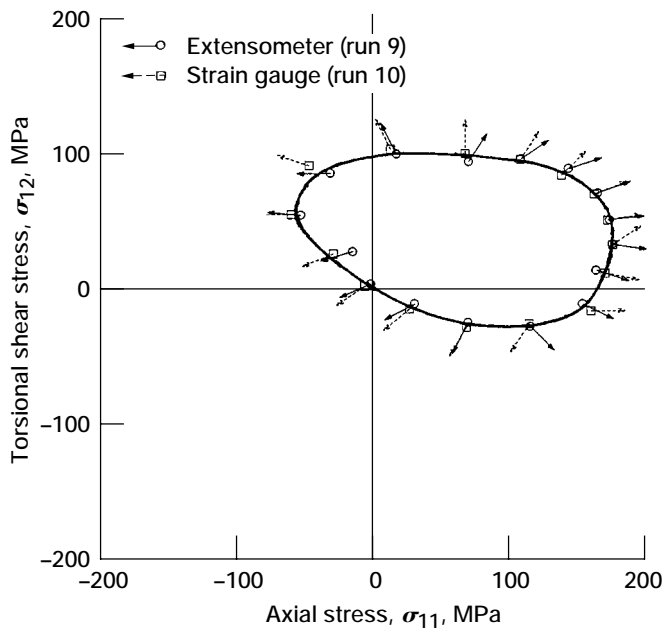
Figure 12.—Direction of inelastic strain increments for 316SS18 after preloading.
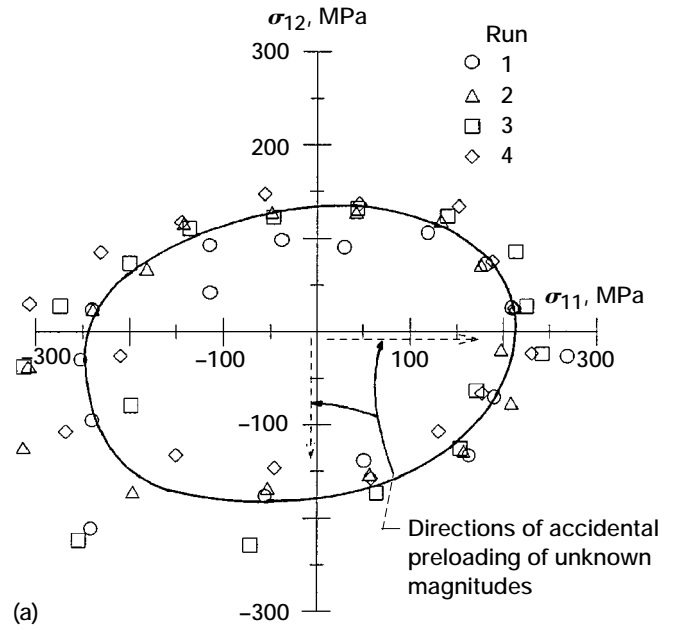
(a)
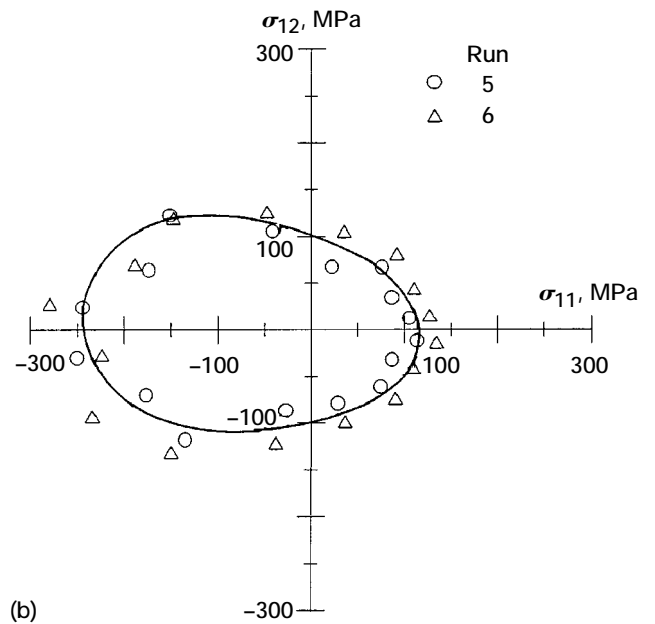
(b)

Figure 13.—Unidirectional W/K yield surfaces at 21 °C. (a) Runs 1 to 4 after preloading. (b) Runs 5 and 6 after heat treatment.
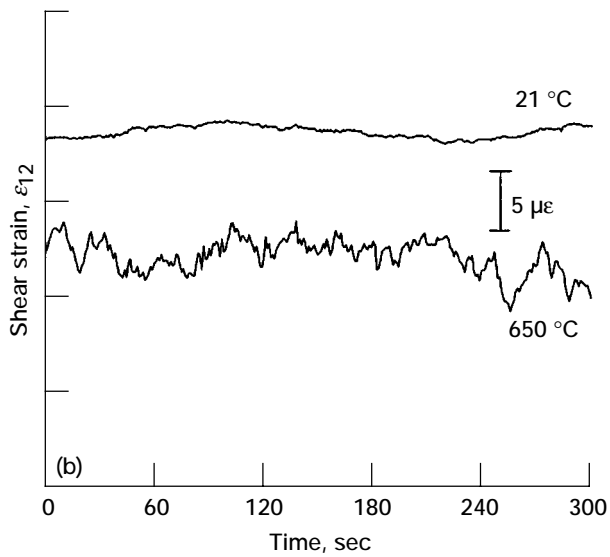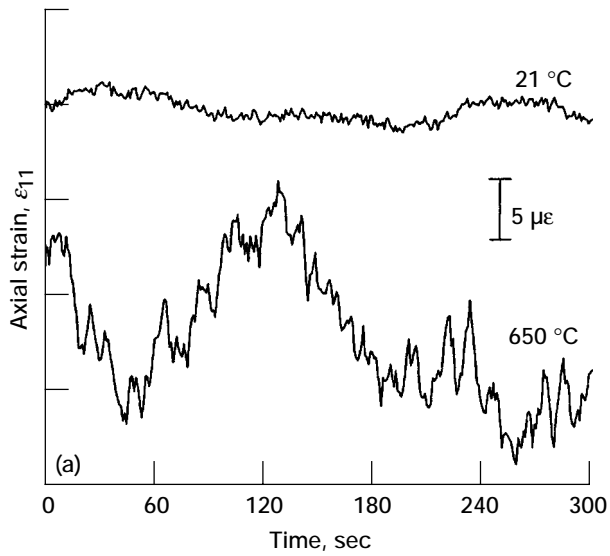
Figure 14.—Extensometer axial and torsional strain signals under zero load for 316 SS. (a) Axial strain ε_{11}. (b) Shear strain ε_{12}.
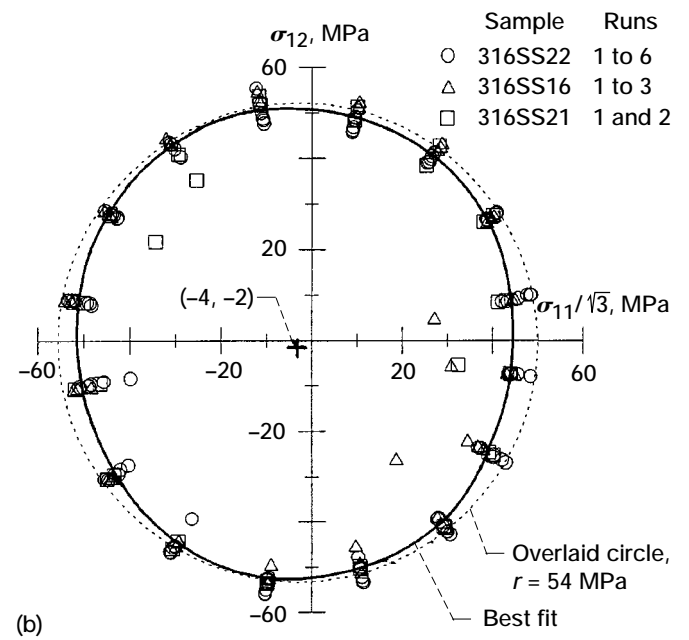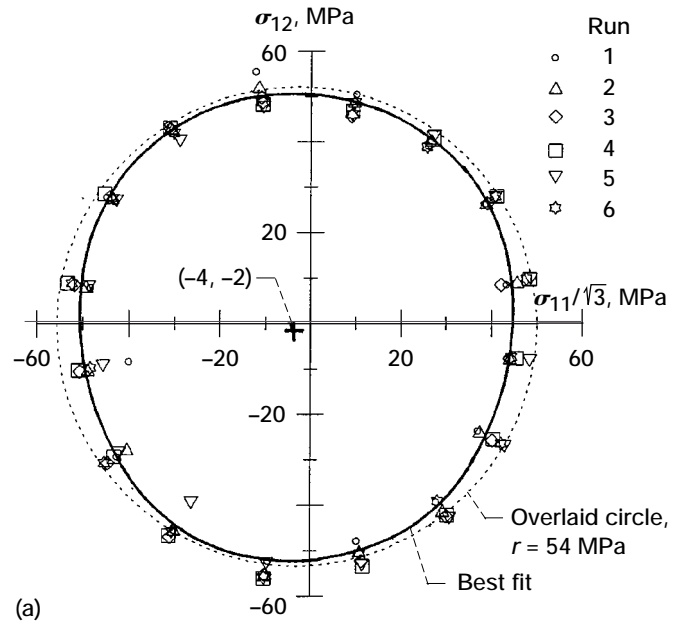

Figure 15.—Initial flow surfaces for 316 SS at 650 °C. (a) Sample 316SS22, runs 1 to 6. (b) Samples 316SS22, runs 1 to 6; 316SS16, runs 1 to 3; and 316SS21, runs 1 and 2.
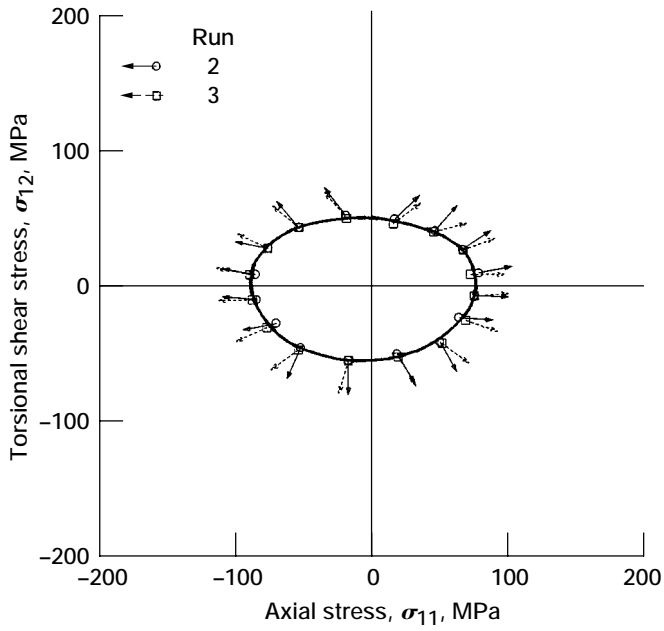
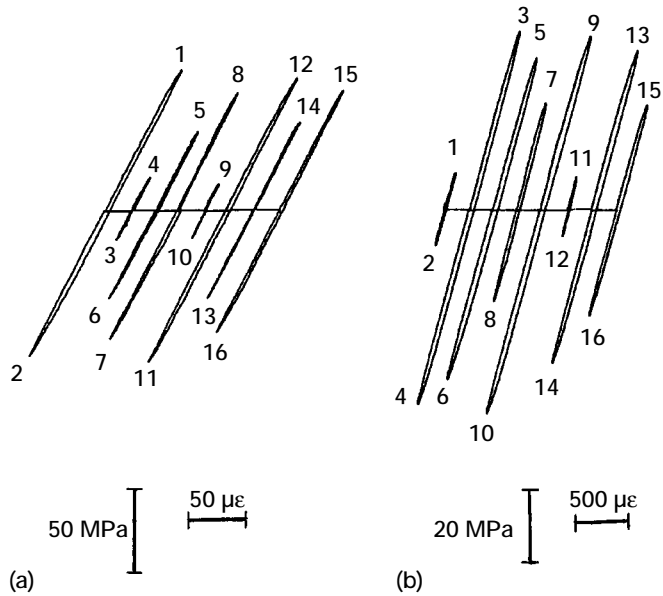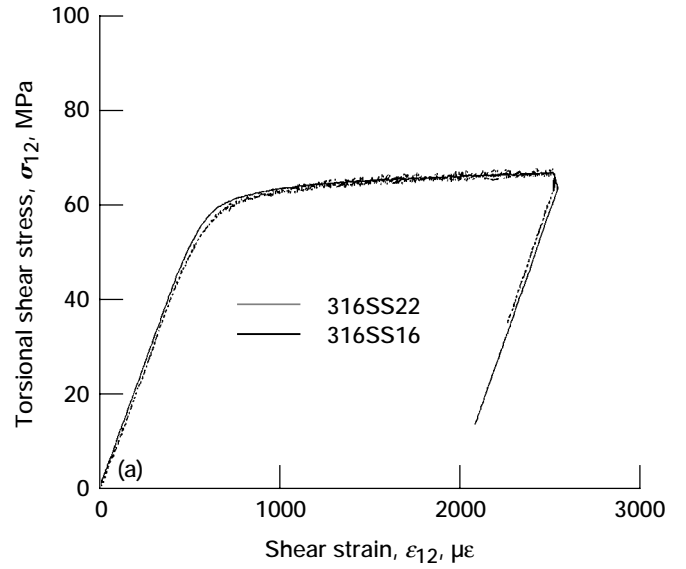Figure 16.—Inelastic strain increments for 316SS22 at 650 °C.

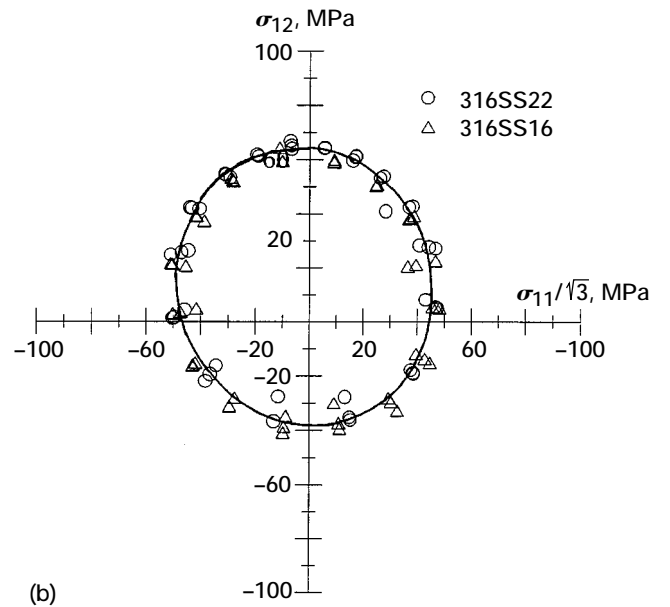Figure 17.—Probe stress-strain responses for 316SS22 (run 4) at 650 °C. (a) Axial. (b) Torsional.

Figure 18.—Preloading and subsequent flow surfaces at 650 °C. (a) Torsional preloading, $\dot{\varepsilon}_e$ = 300 µε/min. (b) Subsequent flow surfaces.

REPORT DOCUMENTATION PAGE

Public reporting burden for this collection of information is estimated to average 1 hour per response, including the time for reviewing instructions, searching existing data sources, gathering and maintaining the data needed, and completing and reviewing the collection of information. Send comments regarding this burden estimate or any other aspect of this collection of information, including suggestions for reducing this burden, to Washington Headquarters Services, Directorate for Information Operations and Reports, 1215 Jefferson Davis Highway, Suite 1204, Arlington, VA 22202-4302, and to the Office of Management and Budget, Paperwork Reduction Project (0704-0188), Washington, DC 20503.

1. AGENCY USE ONLY (*Leave blank*)	2. REPORT DATE	3. REPORT TYPE AND DATES COVERED
	February 1996	Technical Memorandum

4. TITLE AND SUBTITLE

Verification of Experimental Techniques for Flow Surface Determination

5. FUNDING NUMBERS

WU–505–63–12

6. AUTHOR(S)

Cliff J. Lissenden, Bradley A. Lerch, John R. Ellis, and David N. Robinson

7. PERFORMING ORGANIZATION NAME(S) AND ADDRESS(ES)

National Aeronautics and Space Administration
Lewis Research Center
Cleveland, Ohio 44135–3191

8. PERFORMING ORGANIZATION REPORT NUMBER

E–9900

9. SPONSORING/MONITORING AGENCY NAME(S) AND ADDRESS(ES)

National Aeronautics and Space Administration
Washington, D.C. 20546–0001

10. SPONSORING/MONITORING AGENCY REPORT NUMBER

NASA TM–107053

11. SUPPLEMENTARY NOTES

Cliff J. Lissenden, Pennsylvania State University, University Park, Pennsylvania 16802, and Summer Faculty Fellow at Lewis Research Center; Bradley A. Lerch and John R. Ellis, NASA Lewis Research Center; David N. Robinson, University of Akron, Akron, Ohio 44325–3905. Responsible person, Bradley A. Lerch, organization code 5220, (216) 433–5522.

12a. DISTRIBUTION/AVAILABILITY STATEMENT

Unclassified - Unlimited
Subject Category 24

This publication is available from the NASA Center for Aerospace Information, (301) 621–0390.

12b. DISTRIBUTION CODE

13. ABSTRACT *(Maximum 200 words)*

The concept of a yield surface is central to the mathematical formulation of a classical plasticity theory. However, at elevated temperatures, material response can be highly time-dependent, which is beyond the realm of classical plasticity. Viscoplastic theories have been developed for just such conditions. In viscoplastic theories, the flow law is given in terms of inelastic strain rate rather than the inelastic strain increment used in time-independent plasticity. Thus, surfaces of constant inelastic strain rate or flow surfaces are to viscoplastic theories what yield surfaces are to classical plasticity. The purpose of the work reported herein was to validate experimental procedures for determining flow surfaces at elevated temperature. Since experimental procedures for determining yield surfaces in axial/torsional stress space are well established, they were employed—except inelastic strain rates were used rather than total inelastic strains. In yield-surface determinations, the use of small-offset definitions of yield minimizes the change of material state and allows multiple loadings to be applied to a single specimen. The key to the experiments reported here was precise, decoupled measurement of axial and torsional strain. With this requirement in mind, the performance of a high-temperature multi-axial extensometer was evaluated by comparing its results with strain gauge results at room temperature. Both the extensometer and strain gauges gave nearly identical yield surfaces (both initial and subsequent) for type 316 stainless steel (316 SS). The extensometer also successfully determined flow surfaces for 316 SS at 650 °C. Furthermore, to judge the applicability of the technique for composite materials, yield surfaces were determined for unidirectional tungsten/ Kanthal (Fe-Cr-Al).

14. SUBJECT TERMS

Flow surface; Yielding; Composite; Stainless steel; Axial-torsional testing

15. NUMBER OF PAGES

23

16. PRICE CODE

A03

17. SECURITY CLASSIFICATION OF REPORT	18. SECURITY CLASSIFICATION OF THIS PAGE	19. SECURITY CLASSIFICATION OF ABSTRACT	20. LIMITATION OF ABSTRACT
Unclassified	Unclassified	Unclassified	